Video Article

Functional Interrogation of Adult Hypothalamic Neurogenesis with Focal Radiological Inhibition

Daniel A. Lee[1,2], Juan Salvatierra[2], Esteban Velarde[3], John Wong[3], Eric C. Ford[4], Seth Blackshaw[2,5]

[1]Division of Biology, California Institute of Technology

[2]Solomon H. Snyder Department of Neuroscience, Neurology, and Ophthalmology, Johns Hopkins University School of Medicine

[3]Department of Radiation Oncology & Molecular Radiation Sciences, Johns Hopkins University School of Medicine

[4]Department of Radiation Oncology, University Of Washington Medical Center

[5]Institute for Cell Engineering and High-Throughput Biology Center, Johns Hopkins University School of Medicine

Correspondence to: Daniel A. Lee at leed@caltech.edu, Seth Blackshaw at sblack@jhmi.edu

Abstract

The functional characterization of adult-born neurons remains a significant challenge. Approaches to inhibit adult neurogenesis via invasive viral delivery or transgenic animals have potential confounds that make interpretation of results from these studies difficult. New radiological tools are emerging, however, that allow one to noninvasively investigate the function of select groups of adult-born neurons through accurate and precise anatomical targeting in small animals. Focal ionizing radiation inhibits the birth and differentiation of new neurons, and allows targeting of specific neural progenitor regions. In order to illuminate the potential functional role that adult hypothalamic neurogenesis plays in the regulation of physiological processes, we developed a noninvasive focal irradiation technique to selectively inhibit the birth of adult-born neurons in the hypothalamic median eminence. We describe a method for **C**omputer tomography-guided **f**ocal **ir**radiation (CFIR) delivery to enable precise and accurate anatomical targeting in small animals. CFIR uses three-dimensional volumetric image guidance for localization and targeting of the radiation dose, minimizes radiation exposure to nontargeted brain regions, and allows for conformal dose distribution with sharp beam boundaries. This protocol allows one to ask questions regarding the function of adult-born neurons, but also opens areas to questions in areas of radiobiology, tumor biology, and immunology. These radiological tools will facilitate the translation of discoveries at the bench to the bedside.

Video Link

The video component of this article can be found at http://www.jove.com/video/50716/

Introduction

Recent discoveries have demonstrated that the adult mammalian brain can undergo a remarkable degree of plasticity. Adult-born neurons are generated throughout adulthood in specialized niches of the mammalian brain[1]. What is the function of these adult-born neurons? And more so, do they play a role in physiology and behavior? Studies on this topic have traditionally focused on the subventricular zone of the lateral ventricles and the subgranular zone of the hippocampus; however, recent studies have characterized neurogenesis in other brain regions such as the mammalian hypothalamus[2]. Neurogenesis has been reported in the postnatal and adult hypothalamus[2-10], and the function of these newborn hypothalamic neurons remains an active area of investigation.

The functional characterization of adult-born neurons remains a significant challenge for the neuroscience field in general. Selective inhibition of specific neural progenitor populations remains limited by the lack of available molecular markers that are unique to single neural progenitor populations[11]. Thus, selective deletion of adult-born neurons from these neural progenitors via genetic targeting remains difficult. Likewise, viral delivery to target adult-born neurons suffers from potential confounding variables such as introducing injury and inflammation into the environment[12].

New radiological tools are emerging, however, that allow one to circumvent these confounds and investigate these questions through accurate and precise anatomical targeting in small animals. Ionizing radiation inhibits the birth and differentiation of new neurons, and allows a noninvasive method to target neural progenitor populations[13-15]. Recently, we described a germinal region of the mammalian hypothalamic median eminence (ME) that we termed the hypothalamic proliferative zone (HPZ)[2]. We found that when young adult female mice were given a high-fat diet (HFD), levels of neurogenesis in HFD-fed mice were substantially higher than their normal chow (NC) fed controls in this ME region[2]. To test whether adult neurogenesis within the hypothalamic ME regulates metabolism and weight, we sought to disrupt this process. The median eminence is a small unilateral structure at the base of the third ventricle from which regulatory hormones are released. In order to inhibit

proliferation and subsequent neurogenesis without altering the other physiological functions of this brain region, we developed a noninvasive focal irradiation technique to selectively inhibit the birth of newly born adult neurons in the hypothalamic median eminence[2].

A number of groups have employed radiation to suppress neurogenesis in canonical regions[14-28]. However, previous radiological approaches have generally targeted large areas, or often unintentionally also targeted multiple brain areas where neurogenesis has been reported, making it difficult to unambiguously associate any behavioral defects observed with defects in specific neural progenitor populations. The capability for more targeted irradiation is provided by radiological platforms that combine **c**omputer tomography-guided imaging with **f**ocal beam **ir**radiation (CFIR) delivery to enable precise anatomical targeting[29-36]. Radiation beams as small as 0.5 mm in diameter are available to target specific neural progenitor populations[35]. This methodology allows us to target the hypothalamic ME and arrest proliferation and block neurogenesis in small animals. Following radiological treatment on these progenitor populations, physiological and behavioral tests can be performed to illuminate the potential function of adult-born cells. Focal targeting is especially important for our application since the pituitary gland is located close to the hypothalamic median eminence; irradiation of the pituitary may affect hormonal function and subsequently confound results.

The biological basis for the suppression of neurogenesis following irradiation still remains unclear. Previous radiation studies have relied on large area beams, and have concluded that the suppression of neurogenesis is mediated through an inflammatory response[14, 37]. As such it is unclear whether highly focal irradiation could suppress neurogenesis, since it does not evoke a substantial inflammatory response. However, recent studies by our group of the classic neurogenic region in the hippocampus have demonstrated that highly focal irradiation with a dose of 10 Gy can suppress neurogenesis for at least 4 weeks after irradiation[35].

To interrogate the function of adult-born hypothalamic neurons in the median eminence, we use a precision radiation device capable of delivering CT imaging in combination with small-diameter radiation beams to inhibit ME neurogenesis. Using an X-ray tube attached to a gantry that rotates over a range of 360°, we deliver arc-beam micro irradiation beam with the use of a robotically controlled specimen stage that allows rotation of an animal subject during radiation treatment (**Figure 1**). A high-resolution X-ray detector is used to acquire images when the gantry is in the horizontal position[33]. For this study, CT images were reconstructed with an isotropic voxel size of 0.20 mm. On-board CT imaging allowed the identification of a target while the animal is in the treatment position. The target was localized using the CT navigation dose-planning software, which was included with our commercially available radiological platform. After localizing our ROI by CT imaging, the animal was moved to the appropriate treatment position by the robotic specimen stage that has four degrees of freedom (X, Y, Z, θ). Through a combination of gantry and robot stage angles, beams can be delivered from nearly any direction relative to the animal, and stereotactic arc-like treatments are possible[29]. For these and all other imaging studies, the mice were positioned in an immobilization device that allows delivery of anesthetic isoflurane gas while restricting movement. The immobilization bed is CT compatible, and connects to the robotic specimen stage[34].

We expect that CFIR will provide conceptual advances in a number of research areas. Although we use radiological targeting of the hypothalamic median eminence as proof of principle of this technique, CFIR can be used to target any region of the body of any small model organism in principle. In the neurosciences, for example, we envision this technique could be used to evaluate the function of actively proliferative progenitor populations that have been suggested to exist in other circumventricular organs, such as the area postrema[38, 39], subfornical organ[40], and the pituitary[41]. Longstanding controversies regarding the functional role of adult neurogenesis and identifying a causal role in behavior can also now be better addressed. In songbird, this technique might address the role of adult neurogenesis in maintaining the robust and seasonal behavior of birdsong[42], which has been hampered by the ability to selectively inhibit neurogenesis in specific brain regions. Understanding this robust behavioral model might shed new insight into the role of adult neurogenesis in regulating other sexually dimorphic behaviors. Alternatively, in the metabolic field, CFIR might be used to explore aspects of the role of hepatocyte proliferation and its role in metabolism and energy balance. The possibility for conceptual advance in multiple research disciplines is enhanced by the introduction of this technique.

In this paper, we demonstrate the capabilities of CFIR for precision anatomical targeting of a focal irradiation beam. Although we initially developed this small animal radiation research platform (SARRP) for our studies, other similar devices are now commercially available that can accomplish similar CT-guided focal irradiation[43, 44]. Hence, we generalize this CFIR protocol with steps required for all research platforms rather than those specific for SARRP. The advantages of CFIR over previous radiological approaches to inhibit neurogenesis are that this technique allows three-dimensional volumetric image guidance for localization and targeting of the dose, conformal dose minimizes exposure to nontargeted brain regions, and high precision beam geometry allows for conformal dose distribution with sharp beam boundaries. We outline how to use CT-guided imaging to target the dose to a specific anatomical region, and upon doing so, how to visualize the radiation dose distribution directly in tissue using immunohistochemical staining for γ-H2AX, a marker of DNA double-stranded breaks[35, 45-48]. The use of this approach for selective irradiation of neurogenic niches may have significant implications in revealing the functional role of new adult-born neurons on physiology and disease.

Protocol

Animal Usage

Obtain approval from institutional Animal Care and Use Committee for standard care and use protocols. The current protocol was developed for focal irradiation studies on 5.5-10 week old adult C57BL6/J mice, as previously described (**Figure 2**)[2]. However, other ages and small animal species (rats, hamsters, ground squirrels, *etc.*) can also be used, provided that effective anesthesia protocols and a radiographic reference atlas allowing identification of the region of interest (ROI) are available.

1. Calibration of CT-guided Radiological Platform

Perform film-based calibrations for radiation dose on the radiological platform in advance for each collimator size and type of X-ray tube filter used. In order to target an arc beam of irradiation at the desired target site, use the radiation dose-planning software[49] available on most commercial radiation platforms to calculate required delivery time based on the radiation dose, the depth of the region of interest (ROI) based on CT scans of the mouse, and the rotation speed of the robotic platform; details on this are left out of this protocol as they differ between radiation

platforms. For the purposes of visualizing the ventrobasal hypothalamus[2] (**Figure 3**) with CT imaging, operate the X-ray tube with a 0.4-mm focal spot and beam energy of 100 kVp with 1 mm Al filtration. For focal irradiation of the HPZ, operate the X-ray tube at 225 kVp, 13 mA, and a 1-mm focal spot with filtration of 0.15 mm Cu, to deliver 10 Gy of radiation at a tissue depth of 0.6 cm over a treatment time of 4.6 min. Targeting between different ROIs will require calculating different parameters.

1. If studying the effects of high-fat diet on neurogenesis in the median eminence as previously described[2], obtain four-week-old female C57BL6/J mice from Jackson Mouse laboratories, and house four mice per cage. Switch food from normal chow to a high-fat diet at five weeks old. Allow mice to acclimate to new housing and food. Perform CFIR treatment at 5.5 weeks old. Transport subjects to the operation room that contains the radiological platform. Minimize stress levels during transfer. Prepare isoflurane gas anesthesia chamber. Then, add a single mouse into chamber. In parallel, prepare heating pad (low setting) for post-treatment.
2. Once mouse is under and no longer responding to foot-pad compression, bring the subject to the radiological platform and place on the immobilization bed of the robotic stage. Place subject's mouth into the nose-cone anesthesia cup, and teeth into the bite guard (**Figure 1D**). Lay mouse flat on the immobilization bed and check to see if it continues to maintain unresponsiveness. If so, tape down mouse to the bed with gauze tape. While taping down the mouse to the bed, make sure the head is leveled to a horizontal plane. This can be determined by pulling up the ears and seeing if they are leveled. Once the mouse is in the correct position, close the lead protective shield.
3. Acquire the computer-tomography scan using on-board software of the experimenter's radiological platform (this will differ between platforms), which will provide a three-dimensional anatomical structural scan of the mouse subject. Check to see if the mouse head is leveled to the horizontal plane. If not, repeat steps 1.2 - 1.3 until the subject's head is leveled.
4. Identify ROI by CT image. Calculate distance from ROI to the surface of the skull using a 45° angle to the horizontal plane as shown in **Figure 3E**.
5. Using on-board software, take an X-ray of the mouse subject from above as shown in **Figure 4A**. Then, remove mouse from the radiological platform, put on heating pad, and monitor until active.
6. From the coronal CT images, calculate the average ROI anatomical depth of at least three mice in order to determine delivery dosing. As an example from a previous study[2] where 10 Gy of irradiation was administered to the ventrobasal hypothalamus, the depth of the ROI from the skull (from a 45° angle) is 0.66 cm (See **Figure 3E**). Knowing that, the researchers used the dose planning software (DPS) installed on their radiological platform to calculate the appropriate rotation speed and length of treatment to achieve desired dosage to the ROI.
7. After determining treatment duration and rotation speed of the robotic stage with the dose-planning software, measure dose distributions of the calculated parameters with GAFchromic radiation-sensitive films embedded in a water-equivalent plastic mock-mouse model. To do this, embed three GAFchromic radiation-sensitive films between four vertically stacked water-equivalent plastic blocks[29] as shown in **Figure 4B**.
8. Place mock mouse model containing GAFchromic films on robotic stage, and run the focal irradiation beam with the newly calculated parameters. For example, to target the ventrobasal hypothalamus, input the parameters of 0.15 mm Cu filter, 225 kVp, 13 mA, 1-mm diameter radiation beam setting, 45° gantry angle, 1.3°/sec rotation, and 4.6 min to achieve an ROI radiological dose of 10 Gy.
9. Following irradiation, check films for pattern and intensity of radiation dosage. For a 360° angle rotation with the parameters listed to target the ventrobasal hypothalamus, a dark ring in the film above the isocenter, a small crisp spot at the isocenter film, and a lighter ring in the film below the isocenter corresponding to the cone-beam administration of the irradiation will be observed (**Figure 4B**).
10. Superimpose isocenter GAFchromic film over the X-rays of mouse subjects from which the parameters were calculated. The irradiated focal point at isocenter should overlap with the desired ROI region as shown in **Figure 4C**.

Alternative method: If difficulty in targeting brain ROI persists, use iodine contrast injected intrathecally to enhance visualization of ventricles under CT images. For the sake of brevity, this procedure is left out of this protocol, but is previously described[35, 50]. Iodine contrast will provide additional ventricular landmarks (**Figure 5A**).

2. Determining Accuracy of Irradiation Beam

Further confirm CFIR beam accuracy by direct visualization of the radiation beam in tissue[2, 35, 51]. To do this, perform immunohistochemistry to detect γH2AX [51], a histone protein and an early marker of DNA double strand breaks. Mouse subjects must be transcardially perfused and fixed within one hour of irradiation. Following irradiation, DNA repair rapidly ensues, and levels of YH2Ax decrease significantly[35].

1. Repeat steps 1.1 - 1.3.
2. After the target is identified on CT, the mouse subject is moved under robotic control to align this target with the radiation delivery beam. Input calculated parameters (rotation speed and length of treatment to achieve desired dosage) from step 1.6 into dose-planning software and begin treatment. Treatment is delivered with the gantry pointed to 45° from the vertical while the mouse rotates about a vertically-oriented axis.
3. Following irradiation, perform transcardial perfusion on mouse subjects. Perform perfusion within one hour[52]. Following perfusion, immersion fix brains in 4% PFA/PBS and gently rock overnight at 4 °C.
4. The following morning, wash 5 min in PBS 3x to remove paraformaldehyde fixative. Then, immerse in 30% sucrose in 1x PBS on a rocker at 4 °C.
5. Gently rock at 4 °C (usually 12-16 hr), until brain sinks to bottom of tube. This serves as a cryoprotection step. Once brains sink, remove brain with a perforated spoon to prevent excess 30% sucrose/1x PBS transfer. Quickly embed in freezing medium on dry ice. Swirl freezing medium with pipette tip and align brain in plastic mold.
6. Once completely frozen, transfer brain blocks to -20 °C freezer for storage.
7. On the day when immunohistochemistry will be performed, section coronally at 40 µm thickness, and float into a 24-well plate containing PBS with a thin paintbrush. Sections should be kept in correct serial order for immunostaining to determine irradiation coverage of target region.
8. Prewarm 0.01 M sodium citrate solution to 80 °C in water bath in preparation for antigen retrieval step. Simultaneously, while the sodium citrate is warming, perform 5 min washes 3x in 0.01 M PBS.
9. Once sodium citrate solution is at 80 °C, submerge brain sections in the sodium citrate buffer solution. Leave in water bath at 80 °C for 1 hr.
10. Remove section and allow sodium citrate solution to reach room temperature, then perform three 5-minute washes in 0.01 M PBS.
11. Block brain sections for 1 hr in PBS-Triton containing 5% normal goat serum.

12. Incubate brain sections overnight in PBS-Triton containing 5% normal goat serum with 1:700 concentration of mouse anti-phospho-H2AX primary antibody at 4 °C.
13. The next day, perform 15 min washes 3x in 0.01 M PBS-Triton.
14. Incubate brain sections PBS-Triton containing 5% normal goat serum with goat anti-mouse secondary antibody conjugated with 488 nm fluorphore at 1:500 concentration for 2 hr.
15. Perform 15 min washes 3x in 0.01 M PBS-Triton.
16. Perform 4',6-diamidino-2-phenylindole (DAPI) stain (1:5,000 in PBS) for 10 min to visualize nucleus. Then, wash brain sections for 5 min with PBS.
17. Mount on electrostatically charged microscope slides by floating section in PBS. Wipe off excess PBS and allow slides to dry. Coverslip the slides using mounting medium and allow the slides to dry in the dark at room temperature overnight.
18. Take pictures of serial coronal sections with fluorescent microscope. YH2Ax immunostaining (green) indicates site of irradiation. DAPI (blue) is a nuclear stain (**Figure 5B**).

3. Preparation of Mouse Subjects for Focal Irradiation

Examine YH2Ax immunostaining results. Once satisfied with the calibration and targeting of the irradiation beam, proceed with the experiment. At this point, the total time required to treat a mouse (from animal setup to completion of beam delivery) is approximately 10-15 min for a 10-Gy treatment with a 1-mm beam.

1. Order four-week-old C57BL6/J female mice from Jackson Mouse laboratories. House four mice per cage, and switch food from normal chow to a high-fat diet at five weeks old. Ear punch mice to give them unique identifying marks. Monitor health of mice daily. Note: metallic markers cannot be used as they will result in streaking artifacts on the CT.
2. Weigh mice the day before radiation or sham treatment. Split mice into two cohorts for radiation or sham treatment and ensure that there is no significant difference in weight between cohorts. On the day of treatment, when mice are six weeks old, reweigh all mice and record their mass. Gently transport both cohorts to the radiological platform. Take care to minimize stress levels.
3. Prepare isoflurane gas anesthesia chamber. Anesthetize two mice, one in the predetermined irradiation group, and another in the sham control group. Prepare heating pad set in the low setting for postoperative treatment.
4. Follow steps 1.2 - 1.4 for the mouse to receive irradiation. For the sham mouse, keep mouse in anesthesia chamber while treatment is going on. Make sure that anesthesia chamber is near the CFIR platform so any effects on ambient radiation are factored in. After the target is identified on CT, move mouse subject under robotic control to align this target with the radiation delivery beam. Input calculated parameters (rotation speed and length of treatment) into dose-planning software.
5. Once irradiation treatment is complete, return both sham and irradiated mice to heating pad, and monitor until they wake up.
6. Return both sham and irradiated mice to animal facility. Monitor every day. Weigh the mice every half week. To confirm irradiation of targeted hypothalamic proliferative zone, administer intraperitoneal injections of BrdU (50 mg/kg) three days post-treatment and examine neurogenesis between groups by colabeling of immunohistochemistry for BrdU and a neuronal marker one month following initial BrdU exposure (**Figure 6**)[2].

Representative Results

Assessing CT-guided Targeting and Accuracy

The mechanical calibration of the system is critical for ensuring that beams from various angles all intersect in a single point. Calibration was accomplished with a semi-automatic imaging-based method, where end-to-end alignment accuracy has been measured to be 0.2 mm[29]. This accuracy is highly critical as the volume of the hypothalamic median eminence structure is small[2]. To test this calibration, we measured dose distributions with GAFchromic radiation-sensitive films embedded in a water-equivalent plastic mock-mouse model[35] (**Figure 4B**). Briefly, a CT-scan of the mouse subject was taken, and our ventrobasal hypothalamic target site was identified. Delivery and rotation speed were calculated, and the appropriate collimator and filtration were attached to ensure 10 Gy of radiation was delivered. A mock-mouse model designed from a water-equivalent plastic structure embedded with GAFchromic radiation-sensitive films was then substituted for the real mouse subject to measure dose distribution at different focal planes. **Figure 4B** shows end-to-end test results from an arc treatment with the 1-mm-diameter beam using GAFchromic films in a mock-mouse platform. The gantry was set at a 45° angle with respect to the mock mouse model while the robotic specimen stage was rotated around a vertically oriented axis, generating an "arc" or cone of radiation. The full width at half maximum (FWHM) is 2.31 mm, which is larger than 1.0 mm since the arcs impinge on the film at an angle. Theoretically the beam size at this angle should be 2.0 mm. The focal beam spot shown in **Figure 4** demonstrates the precision alignment of beams from different directions. This film can be overlaid on top of the real mouse subject, demonstrating beam position and precision (**Figure 4C**).

Using a 1 mm diameter beam collimator, an arc technique was used to deliver 10 Gy to the target point in our mouse subject. Previous measurements[29] indicate that this technique provides very low doses of radiation (<0.1 Gy) outside the 1 mm target. The area of the pituitary gland and surrounding structures is therefore effectively shielded from focal irradiation of the ventrobasal hypothalamus. The accuracy of the beam targeting has been measured in previous studies to be within 0.2 mm both in phantom tests[29] and tissue sections[35].

While not required, CT-guided targeting of the ROI can be enhanced by an injected intrathecal iodine contrast to enhance CT-guided targeting for our brain application (**Figure 5A**). As this is an invasive and cumbersome procedure, this contrast is not used often, and not described in this protocol. Details for this protocol can be found in Ford *et al.* 2011 and Chaichana *et al.* 2007. The advantages of this iodinated contrast are that the lateral and third ventricles are clearly visualized in CT scans acquired on a CFIR radiological platform (**Figure 5A**). The target was the median eminence, at the base of the third ventricle, and was identified using CT-guided navigation software and automatically imported into the robot positioning interface. Bony cranial structures were identified and used as anatomical landmarks for subsequent studies where iodine contrast was not employed.

Beam Targeting Validation with γ-H2AX

To further confirm our CT-guided targeting of the hypothalamic ME, we visualized the 1-mm irradiation beam in tissue by indirect examination of double-stranded DNA breaks that arise following irradiation. H2AX histone protein is phosphorylated after DNA double-strand breaks. γ-H2AX has been widely used in brain and other tissues[46-48], and the number of γ-H2AX+ foci appears to correlate well with radiation dose over a wide range of doses[51, 53]. We observed clear visualization of the beam following γ-H2AX immunostaining (**Figure 5B**). Resultant γ-H2AX staining showed precise targeting of the expected location. The beam edge was also extremely sharp, in agreement with film-based physics commissioning measurements that indicate a 20-80% penumbra of 0.3 mm[54]. We previously measured the distance between the intended target and the center of the beam as visualized in the tissue sections[35]. The center of the beam was offset from the intended target by a mean distance of 0.19±0.36 mm (standard deviation) in 10 irradiated mice after factoring for effects of tissue shrinkage during fixation and processing[35].

Using a stereotactic-like arc treatment consisting of an arc at 45° from the vertical, we show we were able to effectively target the ventrobasal hypothalamus, without irradiating other neurogenic niches (**Figures 5C-D**). Irradiation of surrounding areas was minimal, and there was a boundary in radiation exposure as demonstrated by GAF-chromic film (**Figure 4B**) and γ-H2AX immunostaining (**Figures 5B-D**). The tissue dorsal to the hypothalamic ME shows light γ-H2AX staining (**Figure 5B**) because the radiation beams enter through this region and also possibly because of enhancement by the overlaying bone even though a relatively hard X-ray beam was used (225 kVp, 0.15 mm Cu filtration).

Effects on Neurogenesis

Upon confirming the specificity of our CT-guided irradiation delivery, we examined the effect of 10 Gy of irradiation on levels of ME neurogenesis. Adult mice were fed a high-fat diet, received the radiation or sham treatment, and then subsequently BrdU injections as previously described beginning at 6 weeks old[2]. Mice were sacrificed for examination at 10 weeks old, one month after the first BrdU injection. Irradiated HFD-fed adult mice exhibited ~85% inhibition of ME neurogenesis compared with sham-treated controls (**Figure 6A**)[2]. The arcuate nucleus, an adjacent structure bordering the irradiation site, was examined for changes in neurogenesis, and found to have no statistically significant difference between irradiated animals and sham controls (**Figure 6A**)[2].

Function of Adult-born Median Eminence Hypothalamic Neurons

Changes in irradiated and sham mice were examined following treatment. Fur coat and response to touch appeared normal. A chemistry panel and complete blood count panel was examined one week following irradiation treatment, and no significant difference was observed (n = 9/group). In high-fat fed mice where we observed a ~85% reduction in adult-born ME neurons one month following irradiation (**Figure 6A**), irradiated mice had decreased weight gain over time compared to the sham treated group (**Figure 6C**). In contrast, normal-chow fed control mice, where observed levels of ME neurogenesis were significantly lower than their high-fat fed counterparts[2], did not have a statistically significant difference in weight between sham versus irradiated groups (**Figure 6B**). Interestingly, this reduced weight gain in irradiated high-fat fed mice is accompanied by changes in metabolism and activity as previously described in detail by our group[2] (**Figures 6D-I**).
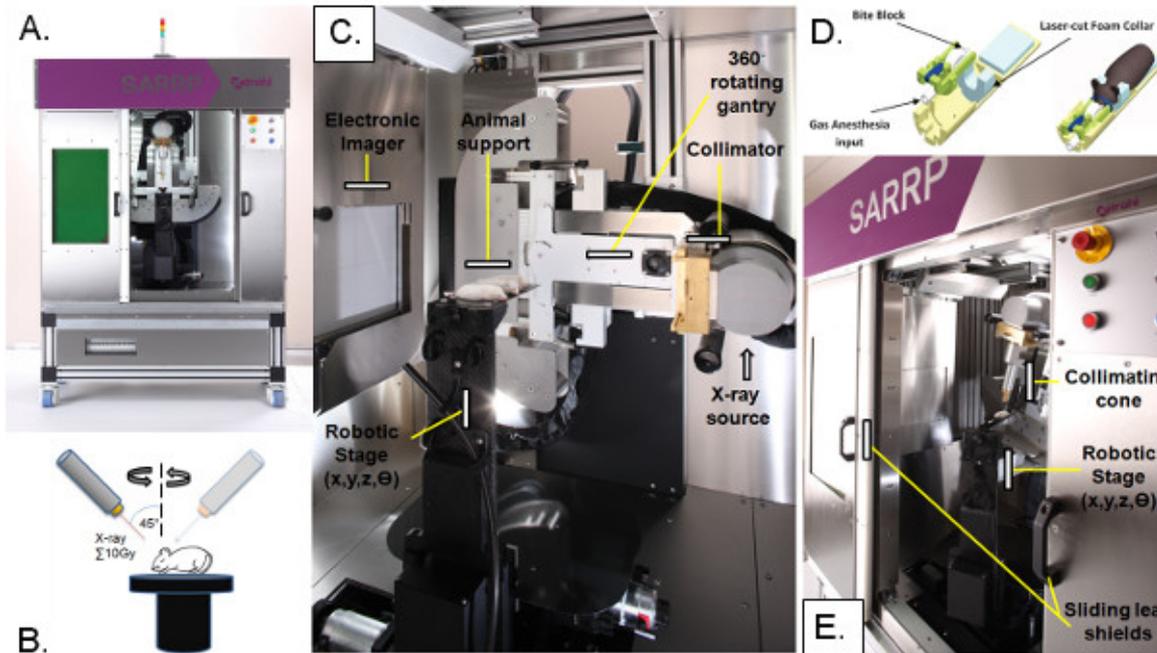
Figure 1. Computer tomography-guided focal irradiation (CFIR) platform. (**A**) CFIR utilizes a precision radiation device capable of delivering CT-guided irradiation with small beams. An example of one CFIR platform is the small animal radiation research platform (SARRP). With lead shielding (as shown), the SARRP stands at 81 inches (height) by 58 inches (width) by 41 inches (depth) at 5,170 pounds. (**B**) Using a dual source X-ray tube attached to a gantry that rotates 360°, the SARRP uses a robotically control specimen stage that allows rotation of an animal subject throughout radiation treatment. (**C**) CFIR hardware is composed of an X-ray source, collimator, rotating gantry, animal support, rotating robotic specimen stage, and electronic imager. (**D**) The mouse subject is placed in an immobilization bed with gas anesthesia input on the robotic specimen stage. From Armour *et al*. 2010. (**E**) CFIR hardware should include customizable collimating cones for focal irradiation delivery of different sizes. Click here to view larger figure.
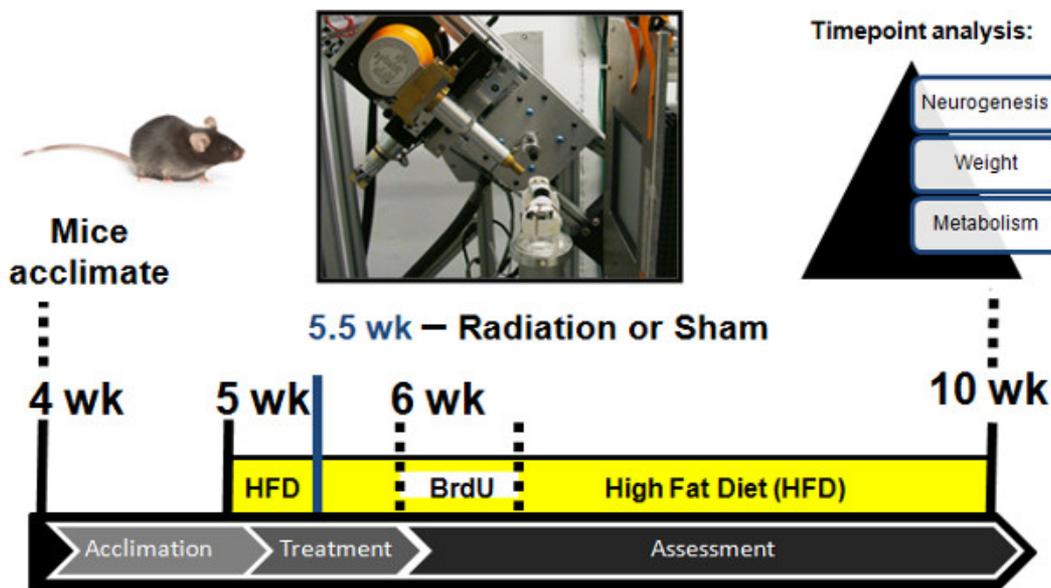

Figure 2. Experimental paradigm. Female C57Bl/6 mice were ordered from Jackson mouse laboratories, and acclimated to resident cages at four weeks old. Mouse subject were switched to an *ad libitum* high-fat diet at five weeks old, and split into two treatment groups: the irradiated or sham cohorts. Physiological assessments were taken longitudinally prior and following treatment. Irradiation or sham treatments were administered at 5.5 weeks. Intraperitoneal BrdU injections were given at six weeks old as previously described[2].
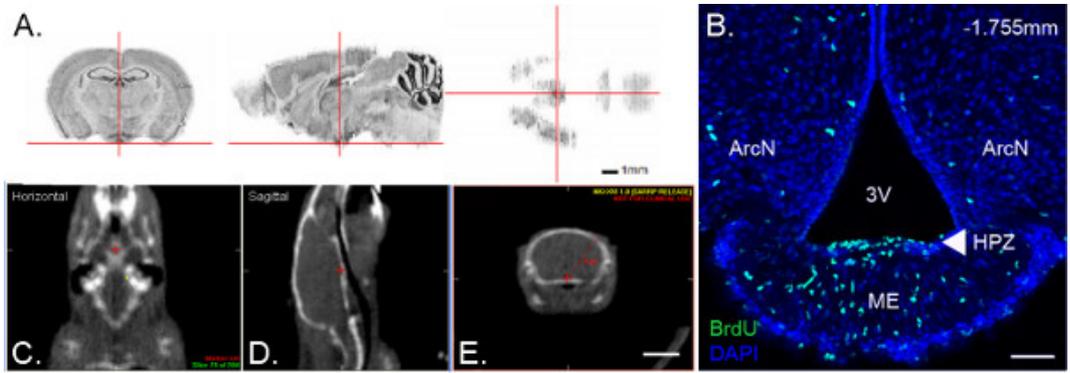
Figure 3. Region of interest localization. The hypothalamic proliferative zone (HPZ), a neurogenic region located in the hypothalamic median eminence, is located in the ventral mediobasal hypothalamus. (**A**) The HPZ region of interest (ROI) is highlighted by red cross-hairs in a 3-D Nissl reference atlas volume from the Allen Brain Atlas Data Portal (position: 7.041, 7.211, 5.564) (available from http://mouse.brain-map.org/)[55]. (**B**) Coronal brain section of the ROI in nineteen-day-old mice. BrdU immunohistochemistry (green) reveals that the ROI (white arrowhead) contains proliferative cells. The density of proliferative cells in the HPZ is restricted in the anterior to posterior axis, with density highest at -1.75 mm Bregma. Tissue sections are counter-stained with DAPI nuclear marker (blue). Figure from Lee *et al.* 2012a. (**C-E**) CT-imaging on a CFIR platform allows targeting the HPZ ROI (red cross-hairs) by arc beam radiation delivery. CT-image of mouse subject in the horizontal plane (**C**), sagittal plane (**D**), and coronal plane (**E**). (**E**) Distance from the surface of the skull to the ROI is 0.62 cm (red line). Scale bars = 1 mm (**A**), 50 μm (**B**), and 0.62 cm (**C-E**). Click here to view larger figure.
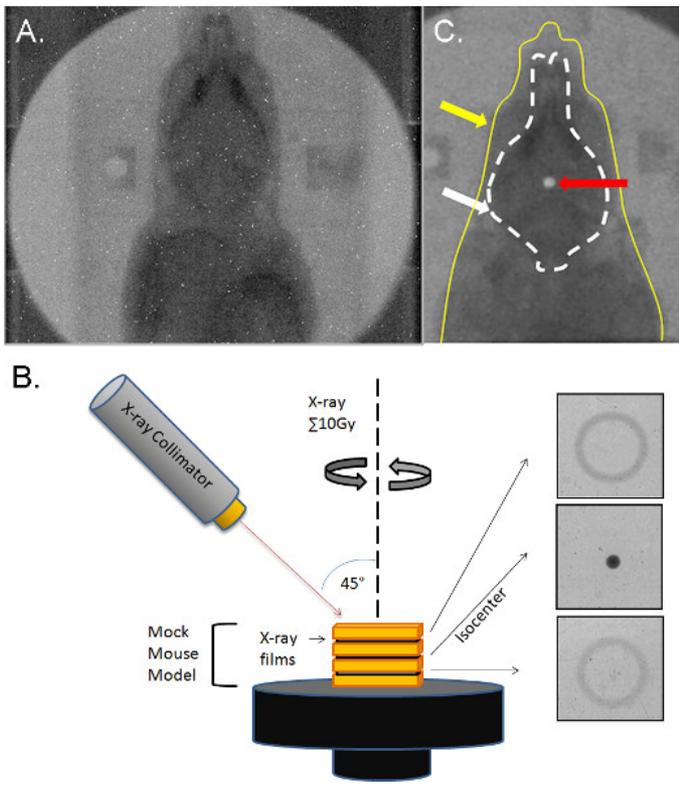

Figure 4. Calibration of irradiation delivery. (**A**) X-ray of a mouse subject secured in the immobilization device on the SARRP robotic stage. (**B**) Calculated ROI coordinates are inputted and targeted against a mock mouse model. The phantom model is composed of GAFchromic radiation-sensitive films embedded in a water-equivalent plastic. Films located above, at, and under the ROI isocenter detect the dose distribution. A 45° arc radiation beam from the SARRP delivers a cone-shaped dose distribution to the ROI, and converges at the isocenter (penumbra spot). (**C**) Superimposition of dosimetry-film acquired with 1-mm radiation beam in phantom with an X-ray of a real mouse subject (yellow line). White circle (arrow) indicates 10-Gy radiation dose focally targeted to HPZ. Dotted line outlines brain. Panel from Lee *et al.* 2012a.
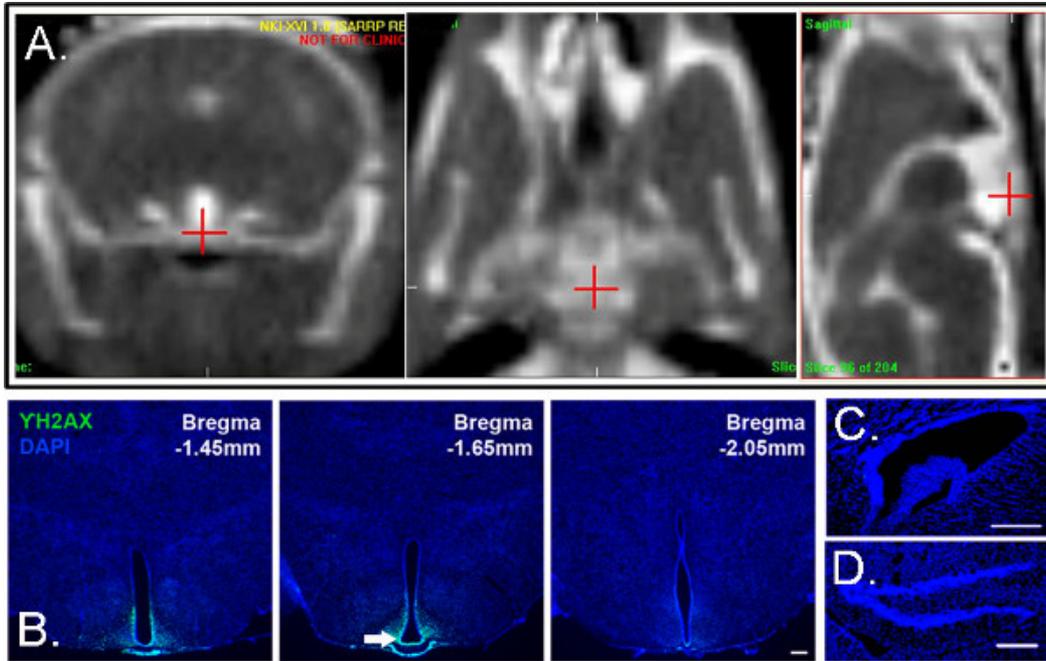
Figure 5. Confirmation of Radiation Delivery. CT imaging with iodine contrast can enhance visualization of the ROI if normal CT imaging does not suffice. (**A**) Mouse subjects received iodine contrasts as previously described (Panel from Lee *et al.* 2012). CT images in the coronal, horizontal, and sagittal plane are shown from left to right. (**B**) Confirmation of radiation delivery in tissue can be detected by immunohistochemistry for γH2AX, a marker of DNA double-stranded breaks. γH2AX immunostaining shows radiation beam delivery targeted to the ROI HPZ in the ventral mediobasal hypothalamus. γH2AX immunostaining is not observed in the subventricular zone of the lateral ventricles (**C**), or the subgranular zone of the hippocampus (**D**) of the same mouse subject. (**B-D**) Sections are counterstained with DAPI (From Lee *et al.* 2012a). Click here to view larger figure.
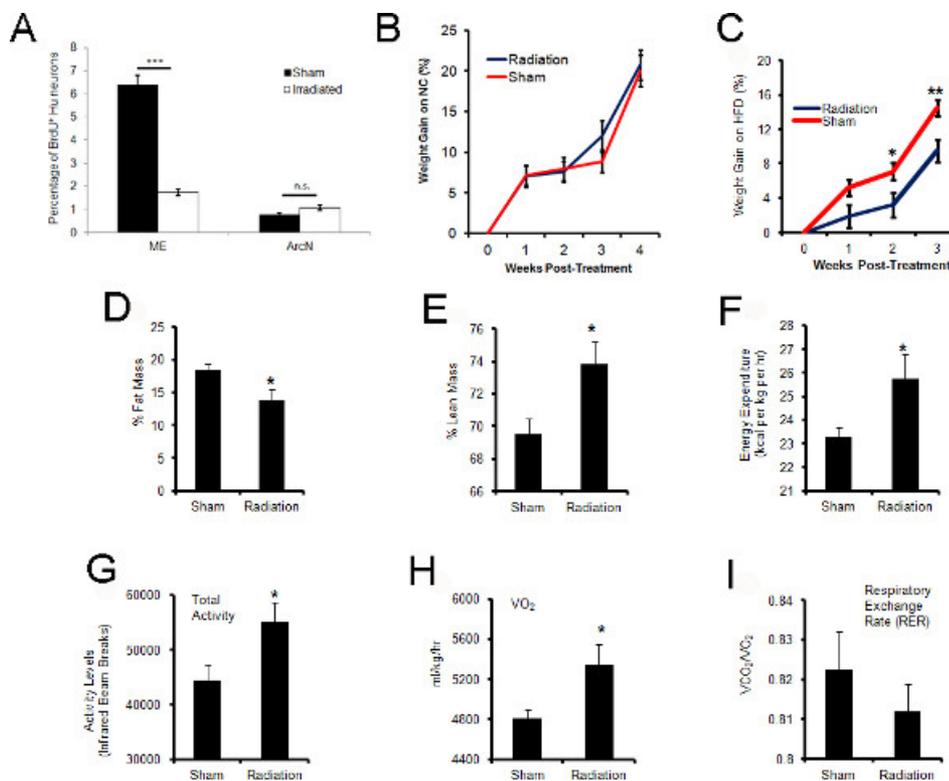
Figure 6. Focal inhibition of ME neurogenesis results in alterations in weight and metabolism. (**A**) The median eminence (ME) located in the ventral mediobasal hypothalamus was targeted for irradiation. The arcuate nucleus (ArcN) is the neighboring anatomical structure. One month following treatment, the percentage of BrdU^{+} Hu neurons from sham versus irradiated cohorts were quantified by immunohistochemistry in the ME and ArcN. Levels of ME neurogenesis were significantly reduced in irradiated versus sham cohorts (n = 5/cohort, *** = p<0.0001). Levels of ArcN neurogenesis were not affected (n = 3/cohort, n.s. = not significant). (**B**) Normal chow fed (NC) and (**C**) high-fat fed (HFD) mice were examined longitudinally for alterations in weight following irradiation or sham treatment (**B**, n = 12/cohort; **C**, n = 9/cohort). (**D-E**) One month following treatment, irradiated and sham treated HFD-fed mice were examined by quantitative magnetic resonance spectroscopy for analysis of % fat mass and % lean mass. Irradiated mice had significantly less % fat mass and significantly more % lean mass than sham controls (n = 5, * = p<0.05). Total mass: (Sham) 21.0±0.3 g, (Irradiated) 18.86±0.4 g; Lean mass: (Sham) 14.6±0.2 g, (Irradiated) 13.9±0.3 g; Fat Mass: (Sham) 3.9±0.2 g, (Irradiated) 2.6±0.3 g (n = 5, * = p<0.05). (**F-I**) Irradiated and sham treated adult mice were placed in a Comprehensive Lab Animal Monitoring System (CLAMS) for simultaneous measurements of food intake, physical activity, and whole-body metabolic profiling two weeks after treatment. Following acclimation in the testing chamber, irradiated mice were observed to have significantly greater energy expenditure, total activity, and VO$_2$ (ml/kg/hr) compared to sham controls during the dark portion of the day (n = 11, 12; * = p<0.05). (**G**) No significant difference was observed in the respiratory exchange rate (RER) (n = 11, 12). Subfigure **A** is generated from data previously published in Lee *et al*. 2012a and Lee *et al*. 2012b. Subfigures **C-I** from Lee *et al*. 2012a . Click here to view larger figure.

Discussion

CT-guided focal irradiation (CFIR) is a novel and complete system approach capable of delivering radiation fields to targets in small animals under robotic control using CT-guidance[32]. The capability of CFIR to deliver highly focused beams to small animal models provides new research opportunities to bridge laboratory research and clinical translation. This paper describes the CFIR approach for precise radiation delivery to specifically target a hypothalamic neural progenitor population. We demonstrate here how to calibrate and confirm radiation delivery specificity via X-ray film and in brain tissue by immunohistochemistry.

In addition, we show how this technique can be used to inhibit neurogenesis in a specific brain region. We demonstrate that we are able to target the ventrobasal hypothalamus, and inhibit neurogenesis in the median eminence, without altering levels of neurogenesis in adjacent structures. Inhibition of ME neurogenesis is accompanied by changes in metabolism and activity, as well as reduced weight gain on a high-fat diet in irradiated versus sham treatment groups (**Figure 6**)[2]. These data suggests a role for these adult-born hypothalamic neurons in regulating metabolism and energy homeostasis. Moreover, it suggests that an excess high-fat diet can alter critical metabolic circuitry even in adulthood[3]. Our results represent an important expansion on the known function of adult-born neurons, and sheds light on a new hypothalamic neural progenitor population[3]. Potential caveats to this approach are that irradiation inhibits progenitor proliferation rather than neurogenesis per se and thus is also possible that physiological changes post-treatment may be partially accounted for by disruption of other adult cell genesis. Future steps will include the development of genetic tools to inhibit the proliferation of this specific neural progenitor population, which will provide substantial clarity to the functional role these progenitors and their progeny play in the regulation of physiology[3].

Taken together, however, this radiological platform serves as an important starting point in performing medium throughput screens on neural progenitors and their progeny. This radiological technique is not limited to research questions in the neurosciences, however, and we expect CFIR to expand the conceptual advance in a number of research disciplines. The recent availability of commercially-sold CT-guided radiological

platforms provides an opportunity for researchers to use these capabilities of this platform for their research questions (**Figure 1**). Several alternatives are commercially available that allow one to perform image-guided small animal irradiation. Furthermore, CT-guided focal irradiation systems can also be built in house, as was the case with the system used for these studies at Johns Hopkins[29-33, 35].

Performing this degree of focal targeting requires proper calibration and targeting of the ROI. While this technique will initially take training in order to become familiar with the CFIR platform and its dose-planning software, operation of the device is rather easy after understanding the protocol and capabilities of the platform. It is recommended that the operator practices calibrating the radiation beam several times prior to running full-scale longitudinal experiment. That said, once fluent in the operation of CFIR, research studies should move quickly.

This CFIR protocol described herein uses three-dimensional volumetric image guidance for localization and targeting of the dose. Conformal dose minimizes exposure to nontargeted brain regions, and high precision beam geometry allows for conformal dose distribution with sharp beam boundaries. This allows one to ask questions regarding the function of adult-born neurons, but also opens areas to questions to the role of cell proliferation in areas such as physiology, tumor biology, and immunology. This method can be expanded in several ways with contrast dyes and bioluminescence to enhance visualization[35, 56]. Efforts are now underway to enhance CFIR hardware capabilities further, and the platform is now being modified to include an on-board positron emission tomography scanner[56]. These will facilitate the expansion of tools available to researchers and aid in translating discoveries at the bench to the bedside.

Disclosures

Acknowledgements

References

1. Ming, G.L. & Song, H. Adult neurogenesis in the mammalian brain: significant answers and significant questions. *Neuron.* **70**, 687-702 (2011).
2. Lee, D.A., *et al.* Tanycytes of the hypothalamic median eminence form a diet-responsive neurogenic niche. *Nat. Neurosci.* **15**, 700-2 (2012).
3. Lee, D.A. & Blackshaw, S. Functional implications of hypothalamic neurogenesis in the adult mammalian brain. *Int. J. Dev. Neurosci.* **30**, 615-21 (2012).
4. Pencea, V., Bingaman, K.D., Wiegand, S.J., & Luskin, M.B. Infusion of brain-derived neurotrophic factor into the lateral ventricle of the adult rat leads to new neurons in the parenchyma of the striatum, septum, thalamus, and hypothalamus. *J. Neurosci.* **21**, 6706-17 (2001).
5. Kokoeva, M.V., Yin, H., & Flier, J.S. Neurogenesis in the hypothalamus of adult mice: potential role in energy balance. *Science.* **310**, 679-83 (2005).
6. Pierce, A.A. & Xu, A.W. De novo neurogenesis in adult hypothalamus as a compensatory mechanism to regulate energy balance. *J. Neurosci.* **30**, 723-30 (2010).
7. Ahmed, E.I., *et al.* Pubertal hormones modulate the addition of new cells to sexually dimorphic brain regions. *Nat. Neurosci.* **11**, 995-7 (2008).
8. Xu, Y., *et al.* Neurogenesis in the ependymal layer of the adult rat 3rd ventricle. *Exp. Neurol.* **192**, 251-64 (2005).
9. Kokoeva, M.V., Yin, H., & Flier, J.S. Evidence for constitutive neural cell proliferation in the adult murine hypothalamus. *J. Comp. Neurol.* **505**, 209-20 (2007).
10. Perez-Martin, M., *et al.* IGF-I stimulates neurogenesis in the hypothalamus of adult rats. *Eur. J. Neurosci.* **31**, 1533-48 (2010).
11. Shimogori, T., *et al.* A genomic atlas of mouse hypothalamic development. *Nat. Neurosci.* **13**, 767-75 (2010).
12. Ming, G.L. & Song, H. Adult neurogenesis in the mammalian central nervous system. *Annu. Rev. Neurosci.* **28**, 223-50 (2005).
13. Limoli, C.L., *et al.* Radiation response of neural precursor cells: linking cellular sensitivity to cell cycle checkpoints, apoptosis and oxidative stress. *Radiat. Res.* **161**, 17-27 (2004).
14. Monje, M.L., Mizumatsu, S., Fike, J.R., & Palmer, T.D. Irradiation induces neural precursor-cell dysfunction. *Nat. Med.* **8**, 955-62 (2002).
15. Wojtowicz, J.M. Irradiation as an experimental tool in studies of adult neurogenesis. *Hippocampus.* **16**, 261-6 (2006).
16. Mizumatsu, S., *et al.* Extreme sensitivity of adult neurogenesis to low doses of X-irradiation. *Cancer Res.* **63**, 4021-7 (2003).
17. Snyder, J.S., Hong, N.S., McDonald, R.J., & Wojtowicz, J.M. A role for adult neurogenesis in spatial long-term memory. *Neuroscience.* **130**, 843-52 (2005).
18. Santarelli, L., *et al.* Requirement of hippocampal neurogenesis for the behavioral effects of antidepressants. *Science.* **301**, 805-9 (2003).
19. Saxe, M.D., *et al.* Ablation of hippocampal neurogenesis impairs contextual fear conditioning and synaptic plasticity in the dentate gyrus. *Proc. Natl. Acad. Sci. U.S.A.* **103**, 17501-6 (2006).
20. Duan, W., *et al.* Sertraline slows disease progression and increases neurogenesis in N171-82Q mouse model of Huntington's disease. *Neurobiol. Dis.* **30**, 312-22 (2008).
21. Rola, R., *et al.* Radiation-induced impairment of hippocampal neurogenesis is associated with cognitive deficits in young mice. *Exp. Neurol.* **188**, 316-30 (2004).
22. Hellstrom, N.A., Bjork-Eriksson, T., Blomgren, K., & Kuhn, H.G. Differential recovery of neural stem cells in the subventricular zone and dentate gyrus after ionizing radiation. *Stem Cells.* **27**, 634-41 (2009).
23. McGinn, M.J., Sun, D., & Colello, R.J. Utilizing X-irradiation to selectively eliminate neural stem/progenitor cells from neurogenic regions of the mammalian brain. *J. Neurosci. Methods.* **170**, 9-15 (2008).
24. Panagiotakos, G., *et al.* Long-term impact of radiation on the stem cell and oligodendrocyte precursors in the brain. *PLoS One.* **2**, e588 (2007).

25. Shinohara, C., Gobbel, G.T., Lamborn, K.R., Tada, E., & Fike, J.R. Apoptosis in the subependyma of young adult rats after single and fractionated doses of X-rays. *Cancer Res.* **57**, 2694-702 (1997).
26. Tada, E., Parent, J.M., Lowenstein, D.H., & Fike, J.R. X-irradiation causes a prolonged reduction in cell proliferation in the dentate gyrus of adult rats. *Neuroscience.* **99**, 33-41 (2000).
27. Tada, E., Yang, C., Gobbel, G.T., Lamborn, K.R., & Fike, J.R. Long-term impairment of subependymal repopulation following damage by ionizing irradiation. *Exp. Neurol.* **160**, 66-77 (1999).
28. Hopewell, J.W., & Cavanagh, J.B. Effects of X irradiation on the mitotic activity of the subependymal plate of rats. *Br. J. Radiol.* **45**, 461-5 (1972).
29. Matinfar, M., Ford, E., Iordachita, I., Wong, J., & Kazanzides, P. Image-guided small animal radiation research platform: calibration of treatment beam alignment. *Phys. Med. Biol.* **54**, 891-905 (2009).
30. Matinfar, M., *et al.* Small animal radiation research platform: imaging, mechanics, control and calibration. *Med. Image Comput. Comput. Assist. Interv.* **10**, 926-34 (2007).
31. Matinfar, M., Iordachita, I., Ford, E., Wong, J., & Kazanzides, P. Precision radiotherapy for small animal research. *Med. Image Comput. Comput. Assist. Interv.* **11**, 619-26 (2008).
32. Matinfar, M., Iordachita, I., Wong, J., & Kazanzides, P. Robotic Delivery of Complex Radiation Volumes for Small Animal Research. *IEEE Int. Conf. Robot. Autom.* **2010**, 2056-2061 (2010).
33. Wong, J., *et al.* High-resolution, small animal radiation research platform with x-ray tomographic guidance capabilities. *Int. J. Radiat. Oncol. Biol. Phys.* **71**, 1591-9 (2008).
34. Armour, M., Ford, E., Iordachita, I. & Wong, J. CT guidance is needed to achieve reproducible positioning of the mouse head for repeat precision cranial irradiation. *Radiat. Res.* **173**, 119-23 (2010).
35. Ford, E.C., *et al.* Localized CT-guided irradiation inhibits neurogenesis in specific regions of the adult mouse brain. *Radiat. Res.* **175**, 774-83 (2011).
36. Redmond, K.J., *et al.* A radiotherapy technique to limit dose to neural progenitor cell niches without compromising tumor coverage. *J. Neurooncol.* **104**, 579-87 (2011).
37. Fike, J.R., Rola, R. & Limoli, C.L. Radiation response of neural precursor cells. *Neurosurg. Clin. N. Am.* **18**, 115-27, x (2007).
38. Bauer, S., Hay, M., Amilhon, B., Jean, A. & Moyse, E. *In vivo* neurogenesis in the dorsal vagal complex of the adult rat brainstem. *Neuroscience.* **130**, 75-90 (2005).
39. Hourai, A. & Miyata, S. Neurogenesis in the circumventricular organs of adult mouse brains. *J. Neurosci. Res.* **91**, 757-70 (2013).
40. Bennett, L., Yang, M., Enikolopov, G., & Iacovitti, L. Circumventricular organs: a novel site of neural stem cells in the adult brain. *Mol. Cell. Neurosci.* **41**, 337-47 (2009).
41. Gleiberman, A.S., *et al.* Genetic approaches identify adult pituitary stem cells. *Proc. Natl. Acad. Sci. U.S.A.* **105**, 6332-7 (2008).
42. Goldman, S.A. & Nottebohm, F. Neuronal production, migration, and differentiation in a vocal control nucleus of the adult female canary brain. *Proc. Natl. Acad. Sci. U.S.A.* **80**, 2390-4 (1983).
43. Chow, J.C., Leung, M.K., Lindsay, P.E., & Jaffray, D.A. Dosimetric variation due to the photon beam energy in the small-animal irradiation: a Monte Carlo study. *Med. Phys.* **37**, 5322-9 (2010).
44. Maeda, A. *et al. In vivo* optical imaging of tumor and microvascular response to ionizing radiation. *PLoS One.* **7**, e42133 (2012).
45. Vasireddy, R.S., *et al.* Evaluation of the spatial distribution of gammaH2AX following ionizing radiation. *J. Vis. Exp.* (42), e2203, doi:10.3791/2203 (2010).
46. Short, S.C., *et al.* DNA repair after irradiation in glioma cells and normal human astrocytes. *Neuro. Oncol.* **9**, 404-11 (2007).
47. Gavrilov, B., *et al.* Slow elimination of phosphorylated histone gamma-H2AX from DNA of terminally differentiated mouse heart cells *in situ*. *Biochem. Biophys. Res. Commun.* **347**, 1048-52 (2006).
48. Nowak, E., *et al.* Radiation-induced H2AX phosphorylation and neural precursor apoptosis in the developing brain of mice. *Radiat. Res.* **165**, 155-64 (2006).
49. Jacques, R., Taylor, R., Wong, J., & McNutt, T. Towards real-time radiation therapy: GPU accelerated superposition/convolution. *Comput. Methods Programs Biomed.* **98**, 285-92 (2010).
50. Chaichana, K.L., Levy, A.P., Miller-Lotan, R., Shakur, S., & Tamargo, R.J. Haptoglobin 2-2 genotype determines chronic vasospasm after experimental subarachnoid hemorrhage. *Stroke.* **38**, 3266-71 (2007).
51. Mah, L.J., *et al.* Quantification of gammaH2AX foci in response to ionising radiation. *J. Vis. Exp.* (38), e1957, doi:10.3791/1957 (2010).
52. Gage, G.J., Kipke, D.R., & Shain, W. Whole animal perfusion fixation for rodents. *J. Vis. Exp.* (65), e3564, doi:10.3791/3564 (2012).
53. Banath, J.P., Macphail, S.H., & Olive, P.L. Radiation sensitivity, H2AX phosphorylation, and kinetics of repair of DNA strand breaks in irradiated cervical cancer cell lines. *Cancer Res.* **64**, 7144-9 (2004).
54. Tryggestad, E., Armour, M., Iordachita, I., Verhaegen, F., & Wong, J.W. A comprehensive system for dosimetric commissioning and Monte Carlo validation for the small animal radiation research platform. *Phys. Med. Biol.* **54**, 5341-57 (2009).
55. Lein, E.S., *et al.* Genome-wide atlas of gene expression in the adult mouse brain. *Nature.* **445**, 168-76 (2007).
56. Tuli, R., *et al.* Development of a novel preclinical pancreatic cancer research model: bioluminescence image-guided focal irradiation and tumor monitoring of orthotopic xenografts. *Transl. Oncol.* **5**, 77-84 (2012).